

Dynamic EFM spectroscopy studies on electric force gradients of IrO₂ nanorod arrays

Daniel (Ching-Shih) Chiang¹, Philip Zifeng Lei¹, Fengyan Zhang²
and Robert Barrowcliff²

¹ School of Engineering and Computer Science, Washington State University Vancouver,
14204 NE Salmon Creek Avenue, Vancouver, WA 98686-9600, USA

² Sharp Labs of America, 5750 NW Pacific Rim Boulevard, Camas, WA 98607, USA

E-mail: chiang@vancouver.wsu.edu

Received 26 October 2004, in final form 6 December 2004

Published 11 January 2005

Online at stacks.iop.org/Nano/16/S35

Abstract

The spectroscopy mode of the electric force microscope (EFM) was used to study the variation of the local electric force gradients above CVD-grown thin films of iridium oxide field emitters. The spacing, radius, and morphology of the nanoprotusions were observed to change significantly within the sample. In this research, we present the first EFM study of the electric force gradients above the iridium oxide (IrO₂) nano-arrays. The electric force gradients are measured with the amplitude change of the EFM cantilever vibration operated in air using the lift-mode technique. Regions in the array with nanorods of largest spacing yield the largest force gradients, but a relatively large non-uniformity of the force gradients is observed. However, relatively homogeneous force gradients were obtained in areas with nanorods of smallest radius and densest population (flower-cluster zone).

1. Introduction

Protrusions at the nanoscale, which include materials such as vertically aligned carbon nanotube arrays, ZnO, In₂O₃, and GaN nanorod arrays have recently been under heavy research for their field emission properties [1–3]. The high aspect ratio of these nanostructures makes them extremely attractive for use as field emitters because they are capable of producing large fields for enhanced electron emission [1]. An immediate application for these field emitting nanoprotusions is in the manufacture of ultra-high-resolution display panels which render them superior to the aging single-electron-gun cathode ray displays [3]. Research on the field emission properties of other materials has also been reported, including Fe, Mo, Si, and Ca nanoprotusion and nanorod arrays [1, 4, 5]. Chalamala *et al* [6, 7] initially reported the field emission characteristics of iridium oxide (IrO₂) tips made by oxidizing the surface of etched iridium (Ir) wires. Their motivation in studying IrO₂ tips was the increased chemical stability that IrO₂ offered over

conventional field emitting refractory materials such as Mo and W. Carbon nanotubes, by comparison, are known to be the best field emitters, which explains their heightened interest for research. Carbon nanotubes have relatively low electron escaping work and very sharp tip curvatures, and remain structurally stable under high electric fields [8]. However, the material properties of IrO₂ can also render them quite attractive for field emitting applications. From the literature, it is found that IrO₂ has a comparable electrical conductivity to its metallic component iridium, which is around 32 μΩ cm [9], but unlike metallic or refractory emitters, IrO₂ is already a stable oxide, making it chemically inert and less susceptible to reactions with oxygen [6]. IrO₂ has also shown to have a low threshold field ($E_{th} \sim 0.7 \text{ V } \mu\text{m}^{-1}$) and a large field enhancement ($\beta \sim 40\,000$), which are comparable to N-doped diamond films and carbon nanotube films [3]. An important property that field emitters must have is emission stability, and it was shown in a previous study that IrO₂ nanorods provided durable emission stability [3].

The variation of electric fields near the tip of IrO₂ nanorods and protrusions are of imperative importance in understanding how they perform as field emitters. The performance of the electric field emitters in an array can depend upon the length, density, spacing, tip diameter, and crystal structure of the IrO₂ nanorods. Jo *et al* [10] have previously studied these parameters in carbon nanotube (CNT) arrays. They discovered that in a CNT array with nanotubes of a certain length the threshold electric field, which is the electric field when the emission current density reaches 1 mA cm⁻², decreased as the spacing between the nanotubes was increased. Moreover, in CNT arrays with nanotubes of a certain spacing, the threshold electric field decreased as the length of the tubes was increased [10]. Ba *et al* [8] used an electrostatic force microscope (EFM) to measure the local electric field of a CNT array by means of detecting and recording the electrostatic force gradients above the sample. They determined that differences in CNT height and density have a pronounced effect in the uniformity of the electric fields produced near the emitter surface [8]. Consequently, in this study, electrostatic force gradients in IrO₂ arrays of different nanorod density, spacing, and morphology were investigated using the EFM.

The application of a bias voltage to an IrO₂ nanorod array produces electric field gradients, which induces the creation of long-range electrostatic force gradients in the space above the IrO₂ nanorod tips of the array. The magnitude of these long-range electrostatic forces can be detected and measured with the use of an EFM. The EFM is an extension of the atomic force microscope (AFM) of which a conductive cantilever is oscillated near its resonance frequency at a certain specified height above the sample. In this way, the long range electrostatic forces above the sample can interact with the free vibrating cantilever, thus changing the cantilever's vibration amplitude. From the literature, the AFM and its family of microscopes have been shown to be extremely useful tools in measuring forces with high spatial resolution [7]. The EFM is capable of detecting the electrostatic force gradients produced by the electric field from the biased sample. These force gradients are proportional to changes in the oscillation amplitude or phase of the cantilever vibration. The EFM is an appropriate detection technique for electrostatic forces of IrO₂ nanoprotusions because the instrument has the capability of detecting force gradients as small as 3×10^{-6} N m⁻¹ [7]. For example, researchers have successfully used the EFM to detect the presence of dielectric material over silicon, to measure the voltage in a p-n junction with sub-micron spatial resolution, and to image the voltage distribution over highly integrated chip circuits [7, 11].

In this paper, we provide an EFM study on the electrostatic force gradients of IrO₂ nanorods grown in a CVD chamber. The CVD grown IrO₂ nanorods produce vertically aligned arrays with high diameter to length aspect ratios, increased morphology repeatability, and the capability of producing arrays with nanorods of different spacings and densities.

2. IrO₂ nanorod synthesis and properties

The IrO₂ nanorods were grown on a silicon(100) substrate coated with a titanium (Ti) film. The titanium film serves as a growth promotion layer for the IrO₂ nanorods.

Catalyst particles comprising of (methylcyclopentadienyl) (1,5-cyclooctadiene) iridium were then evenly placed on the titanium coated silicon substrate and inserted into a chemical vapour deposition chamber (CVD) to undergo the growing process. The CVD chamber is purged with oxygen until it reaches a pressure of 30–50 Torr. The CVD chamber's deposition temperature was set to 300–400 °C. This CVD process produces nanorods aligned in close proximity with each other, thus forming arrays. The IrO₂ nanorods were found to have diameters ranging from 50 to 100 nm with average lengths of approximately 250 nm. The reference for the synthesis of IrO₂ nanorods will be published in [18].

3. The electrostatic force microscope (EFM)

For EFM, an NT-MDT Solver Uni SPM system was used in conjunction with tungsten carbide (WC₂) coated silicon cantilevers. The metallic coating enables the cantilever to be conductive and thus be biased or grounded. In these experiments, the cantilever was grounded while applying a bias voltage of –6 and –9 V to the sample's titanium film.

The EFM measurement technique performed on the IrO₂ nanorods was the spectroscopy mode. In spectroscopy mode, the cantilever is first approached to the sample surface using the tapping mode and then removed a large distance away from the sample until the cantilever reaches free oscillation. The cantilever's oscillation amplitude is continuously measured as it travels away from the sample. This method permits changes in electrostatic force gradients to be measured as a function of the sample to tip separation distance Z .

3.1. Theory of EFM

During EFM, when a force gradient is present, the gradient interacts with the tip, producing a change in the spring constant, k , which in turn shifts the oscillation resonance frequency of the cantilever [12, 13, 17]. This shift in the oscillation resonance frequency produces a change in the oscillation amplitude, which is detected by the AFM's laser and photodiode sensors as a decrease in the oscillation amplitude of the cantilever.

The sensitivity of the EFM can be increased by setting the cantilever to oscillate at a driving frequency value close to its resonant frequency; more precisely, it is set to oscillate at the steepest section of the amplitude versus oscillation frequency plot. The driving frequency, ω_{dr} , at the steepest section is given by the equation

$$\omega_{dr} = \omega_0 \left(1 + \frac{1}{\sqrt{8}Q} \right) \quad (1)$$

where ω_0 and Q are the resonant frequency and quality factor of the cantilever, respectively. This technique of using a driving frequency at the steepest section of the amplitude versus oscillation frequency plot is called the slope technique [14]. Setting the driving frequency at ω_{dr} permits the cantilever to undergo a maximum change in oscillation amplitude when there is a shift in the resonant frequency of the cantilever [14]. By knowing the change in oscillation

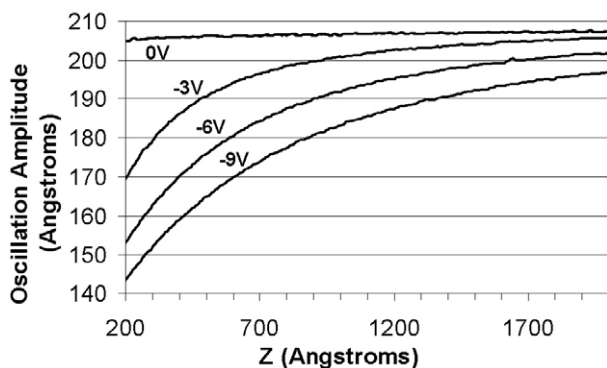


Figure 1. Plot showing spectroscopy data of an individual IrO₂ rod obtained at various bias voltages applied to the sample. The plot shows the change in the oscillation amplitude of the cantilever due to the presence of a force gradient as it travels away from the nanorod.

amplitude, the electrostatic force gradients, dF/dZ , can be computed with the following equation:

$$\frac{dF}{dZ} = \frac{3\sqrt{3}(\Delta A)k}{-2QA_0} \quad (2)$$

where ΔA is the change in oscillation amplitude of the cantilever, k is the spring constant of the cantilever, Q is the quality factor, and A_0 is the free oscillation amplitude at resonance frequency [11]. We find that the WC₂ coated silicon cantilevers have an average quality factor, Q , of around 300, and an average resonance frequency of 285 kHz. The spring constant of the cantilevers given by the manufacturer has a typical value of $k = 11.5 \text{ N m}^{-1}$. The sample was only tested with a negative bias because Liang *et al* [15] observed that the oscillation amplitude only reacts to the magnitude of the applied voltage and it is independent of the polarity. We were also able to confirm this observation in our experiments.

3.2. Experiment

First, an image of the topography was obtained by means of the tapping-mode AFM. After the acquisition of an initial image, we can proceed in collecting spectroscopy data. The spectroscopy data consist of measuring the oscillation amplitude versus tip to sample separation distance, Z . The tip is lifted a distance of over 3000 Å from the sample, and the tip's oscillation amplitude is measured at preset intervals during its travel along Z . The spectroscopy measurements were carried out with the driving frequency set to ω_{dr} in equation (1), and the cantilever free oscillation amplitude was set from 15 to 30 nm. An electrostatic force was induced by applying a bias voltage to the sample while keeping the cantilever grounded. We performed spectroscopy on IrO₂ individual rods at various population densities, and on clusters of intermingled rods for comparison purposes. Figure 1 shows the spectroscopy curves of an individual IrO₂ rod acquired at 0, -3, -6, and -9 V applied to the sample.

With the application of a bias voltage, the electrostatic force gradients are present and therefore interactions of the forces with the tip are detectable and are manifested as a change in oscillation amplitude. The spectroscopy curves from figure 1 show that as the bias voltage is increased there is an

increase in the electrostatic force gradients, which causes an increase in the change of oscillation amplitude of the cantilever. In short, the higher the applied bias, the greater the electrostatic force gradients, the larger the decrease in oscillation amplitude. However, the bias voltage should produce electrostatic force gradients much smaller than the spring constant, k , of the EFM cantilever.

Usually, a thin moisture layer is present in all surfaces exposed to ambient air conditions. We performed cantilever deflection versus Z spectroscopy with the AFM to determine the thickness of this moisture layer. From deflection spectroscopy, the moisture layer was found to have an effect on the cantilever until approximately 25 nm away from the sample. Therefore, all data points below a Z of 30 nm were omitted during electric force gradient calculations.

4. Results

The SEM was first used to analyse the morphology, density, and structure of the CVD grown IrO₂ nanorod arrays. It was found that different regions exist within the same sample. After the initial SEM inspection, EFM spectroscopy measurements were performed on the IrO₂ sample. The resulting force gradients dF/dZ acting on the cantilever were calculated from the changes in oscillation amplitude of the EFM cantilever.

4.1. Morphology of IrO₂

Figure 2 shows SEM images of the IrO₂ nanorod arrays, and figure 3 is AFM tapping-mode images. From SEM micrographs, it is indicated that different regions of the array exist. These regions have different IrO₂ nanorod population densities. Figures 2(a)–(c) depict the densest, medium-dense, and least-dense populated areas of the array. The nanorods in these three regions are found to be similar in shape and structure. Their average measured height is in the order of 200–300 nm, and the nanorods are clearly individually separate from each other; we named the nanorods in these regions ‘regular’ IrO₂ nanorods. On the other hand, notice that from figure 2(d) an extremely dense region was imaged with the presence of large clusters. These clusters have nanoprotusions and rods stuck to each other, producing a flower-like pattern. The petal-like structures appear to be formed by IrO₂ nanorods of various shapes and sizes. We call this structure IrO₂ flower clusters due to its shape. Figure 3 shows AFM images of the corresponding dense, least-dense, and flower-cluster regions in the IrO₂ nanorod array. From figure 3(c), the IrO₂ flower clusters are perceived by the AFM as large bright boulders.

It is not yet conclusive as to why density variations of nanorods exists in a single sample, but it is speculated to be caused by two synthesis factors which happen before undergoing reaction in the CVD chamber. These factors are attributed to the uneven distribution of the catalyst compounds on the titanium coated (100) silicon surface, and the non-uniform deposition of the titanium growth promoting layer on the (100) silicon.

4.2. EFM spectroscopy

As explained in previous sections, EFM spectroscopy basically consists of measuring the change in oscillation amplitude as a

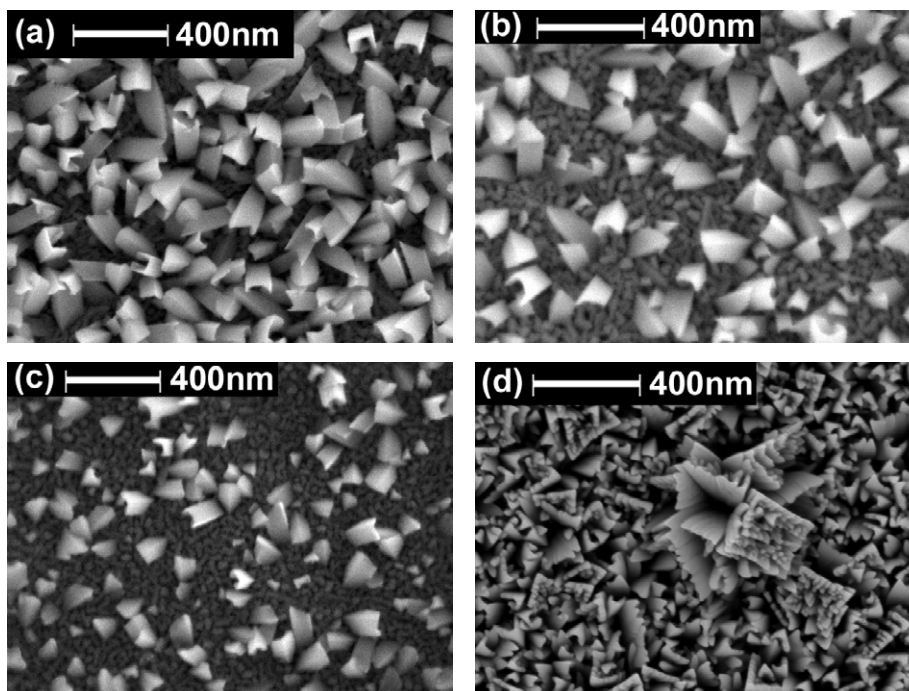


Figure 2. SEM micrographs of CVD produced IrO_2 nanorod arrays. There are four different regions. (a) Densely populated array with regular shaped IrO_2 nanorods. (b) Medium-dense array with regular shaped IrO_2 nanorods. (c) Least-dense array with regular shaped IrO_2 nanorods. (d) Densely populated IrO_2 nanorod array with flower shaped clusters. Notice the shorter nanorod heights in the least-dense area. The nanorod arrays with the flower clusters have smaller diameters and are vertically well aligned.

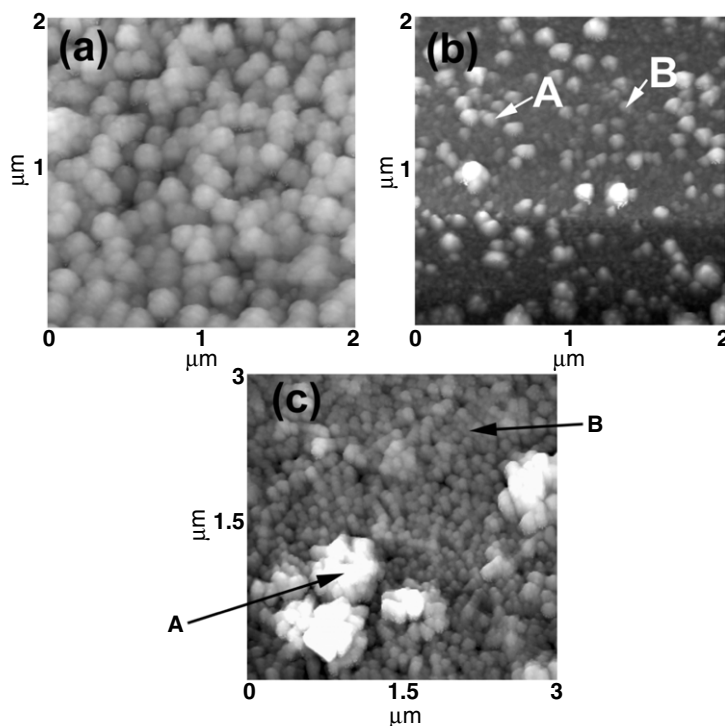


Figure 3. AFM images of CVD produced IrO_2 nanorod arrays in the following regions: (a) densely populated nanorod array with regular shaped IrO_2 nanoprotusions, (b) least-dense nanorod array with regular shaped IrO_2 nanoprotusions (notice the shorter and less regular shaped nanorods), and (c) densely populated IrO_2 nanorod array with flower shaped clusters. The flower clusters are imaged as large bright boulders by the AFM, and the regular nanorods are the protrusions surrounding the flower clusters.

function of sample–tip separation distance Z . The electrostatic force gradients were calculated from the change in amplitude of the cantilever and are graphed in a log–log plot. For a sample

biased with -6 V, the change in amplitude is calculated by subtracting the spectroscopy curve measured at -6 V from the spectroscopy curve measured at 0 V. Then equation (2) is used

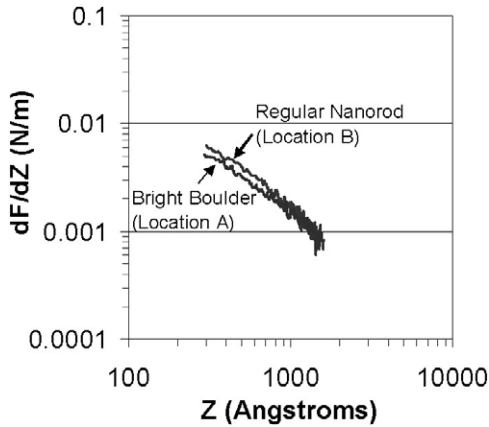


Figure 4. Plot of force gradient versus sample–tip separation distance, Z , of regular IrO₂ nanorods (location B of figure 3(c)), and bright boulder IrO₂ nanorods (location A of figure 3(c)). The sample was biased with -6 V. Note that the measured electrostatic force gradients are similar in magnitude.

to obtain the magnitude of the electrostatic force gradients. We started by performing EFM spectroscopy on IrO₂ flower clusters and regular IrO₂ nanorods. This was done to compare how electrostatic force gradients vary from regular nanorods to flower-cluster nanorods in the array. A bias of -6 V was applied to the samples. Figure 4 shows the log–log plot of the measured electrostatic force gradients of the bright boulder (location A in figure 3(c)) and regular regions (location B in figure 3(c)) in the flower-cluster region as a function of Z . As expected, the magnitude of the force gradient decreased as the sample to tip separation, Z , increased.

It is evident from figure 4 that the electrostatic force gradients of the IrO₂ nanorods measured above location A appear to be very close in magnitude to those of the regular nanorods in location B. This can be due to the fact that nanorods in this flower-cluster region are quite densely populated, have smaller diameters, and are less tilted, thus giving them equally viable field enhancement properties. Due to the high packing density of nanorods in the flower-cluster region, variations in the spacing, radius, and length of the nanorods do not have a large effect on the overall field enhancement properties of the array. Therefore, the electrostatic force gradients are fairly uniform throughout the nanorod flower clusters. Observations of similar results were also reported from studies of densely packed CNT arrays by Jo *et al* [10].

The variations of force gradients among IrO₂ nanoprotusion arrays of different densities were also investigated by performing EFM spectroscopy on the different regions of the sample accordingly. Data were collected from the densest and least-dense populated regions. The sample was applied with a bias voltage of -6 V. The average of electrostatic force gradients versus Z was calculated from the collected data of several points in the same region and graphed on a log–log plot found in figure 5. It was observed that the force gradients detected in the densest area are comparably smaller than those in the least-dense area. The decreased measured electric force gradients in the densest region of the IrO₂ array can be attributed to the fact that the IrO₂ nanorods are extremely close to each other, thus its field-enhancement factors are a lot smaller because the electric field from one rod is screened and disrupted by the electric

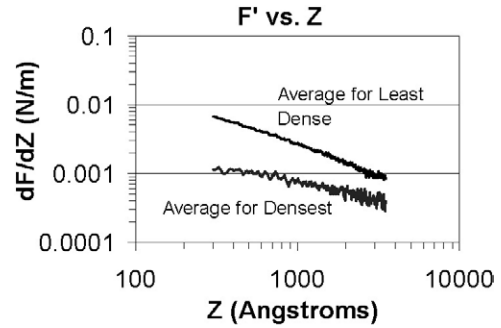


Figure 5. Plot of the averaged force gradient versus sample–tip separation distance in IrO₂ arrays of different densities. A bias of -6 V was applied to the sample. The areas with densely populated nanoprotusions were observed to produce the lowest force gradients whereas the least-dense populated areas yield larger force gradients.

field from neighbouring nanorods [10, 16]. This phenomenon was observed by Jo *et al* [10] in studies on the field emission properties of vertically aligned carbon nanotubes. It was determined from CNT arrays that the relationship between the electric field-enhancement factor, γ , and the length and spacing of the CNTs can be given by

$$\gamma = \gamma_0 \left[1 - \exp\left(\frac{-2.3172s}{l}\right) \right] \quad (3)$$

where γ_0 is the intrinsic field-enhancement factor of the CNTs, s is the spacing between tubes, and l is the length of the CNTs. Note that γ_0 is a function of the radius of the CNTs ($\gamma_0 \propto 1/r$) [10]. It is observed that IrO₂ nanorod arrays also follow a similar relationship between nanorod radius, spacing, and field-enhancement factor given by equation (3). From figure 2, the SEM micrographs show that the least-dense region of the IrO₂ array has a large spacing between nanorods and smaller nanorod radiuses, which according to equation (3) results in larger field enhancement.

EFM spectroscopy measurements at different points can provide a look at the local electric field gradients within each region of the IrO₂ nanorod array. Spectroscopy data collected from the different points in the same region suggest that the local electrostatic force gradients do not remain constant. Rather, the local electrostatic force gradients change from one location to another within each region. Figure 6 shows the spectroscopy curves of two different locations A and B that are 700 nm apart from each other (these can also be found in figure 3(b) as locations A and B). The spectroscopy curves were acquired within the least-dense region of the IrO₂ array. The sample was biased with -9 V during the EFM spectroscopy measurements. Again, from figure 6, it is quite apparent that differences exist between the spectroscopy curves obtained at different locations within the same region. The question one might ask is what causes this variation in local electrostatic force gradients. Although not yet conclusive, the variation in local electrostatic force gradients is a phenomenon that can be attributed to the actual structure of the IrO₂ nanorods. For example, it has been readily seen from SEM micrographs that not all of the IrO₂ nanorods are aligned vertically up at a 90° angle with the substrate (figure 2). There is usually a certain tilt, which appears to drastically increase as the nanorod array becomes less and less dense. The least-dense regions of the

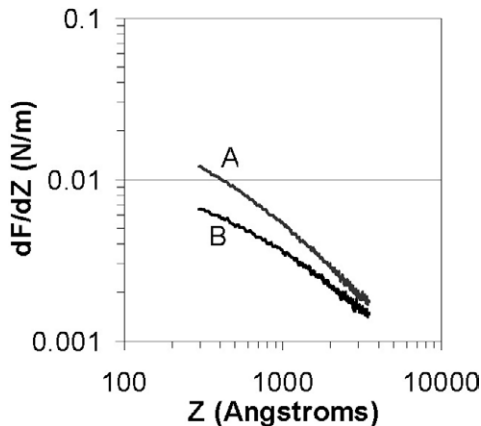


Figure 6. EFM spectroscopy curves obtained at two different locations A and B of figure 3(b) in the region with least-dense IrO₂ nanorod population. A bias of -9 V was applied to the sample. The spectroscopy curves for locations A and B were measured at a distance of approximately 700 nm away from each other. Notice that even within the same region, different values of the local electrostatic force gradients are measured.

IrO₂ nanorod array appear to have the most tilt. If the nanorod is tilted, the nanorod tip will not only have a vertical electric field component, but will also contribute to the lateral field, which might affect the measured magnitude of the electrostatic force gradients even in the same region of a nanorod array.

5. Conclusions

In summary, the electrostatic force gradients in IrO₂ arrays with nanorod population densities from the densest, the least-dense, and the flower-like cluster regions were studied with the EFM. The magnitudes of the electrostatic force gradients change in these three typical areas of the IrO₂ nanorod array. The EFM spectroscopy data indicated that the regions with the least-dense population of nanorods yielded the largest force gradients whereas the densest regions yielded a lower force gradient. The force gradient within the least-dense zone and the densest zone is relatively non-uniform ($>40\%$). The variation of the force gradient in the flower-cluster zone is much smaller ($<10\%$) compared to those of the other zones, which implies that the most homogeneous electric field distribution might be located in the flower-cluster areas.

Acknowledgments

The authors would like to thank Dr Xiaolin (Linda) Chen of the Mechanical Engineering Department at Washington State University Vancouver for her helpful comments, discussions, and critical review of the manuscript.

References

- [1] Kim D-H *et al* 2004 Field emission properties of vertically aligned iron nanocluster wires grown on a glass substrate *Appl. Phys. Lett.* **85** (1)
- [2] Jo S H *et al* 2004 Field emission of zinc oxide nanowires grown on carbon cloth *Appl. Phys. Lett.* **85** (8)
- [3] Chen R-S *et al* 2004 Field emission from vertically aligned conductive IrO₂ nanorods *Appl. Phys. Lett.* **84** 1552
- [4] Rudolphi M and Markwitz A 2004 *Appl. Phys. Lett.* **85** (15)
- [5] Zhao X *et al* 2004 *Appl. Phys. Lett.* **85** (8)
- [6] Chalamala B R, Wallace R M and Gnade B E 1998 *J. Vac. Sci. Technol. B* **16** 2859
- [7] Chalamala B R *et al* 2002 Field emission characteristics of iridium oxide tips *J. Appl. Phys.* **91** (9)
- [8] Ba L *et al* 2003 Probing local electric field distribution of nanotube arrays using electrostatic force microscopy *J. Appl. Phys.* **93** (12)
- [9] Ryden W D, Lawson A W and Sartain C C 1970 *Phys. Rev. B* **1** 1494
- [10] Jo S H *et al* 2003 Effect of length and spacing of vertically aligned carbon nanotubes on field emission properties *Appl. Phys. Lett.* **82** (20)
- [11] Said R A 2001 Perturbation detection of electric force gradients using the phase shift method *J. Phys. D: Appl. Phys.* **34** L7–10
- [12] Albrecht T R, Grutter P, Horne D and Rugar D 1991 Frequency modulation detection using high-Q cantilevers for enhance force microscope sensitivity *J. Appl. Phys.* **69** (2)
- [13] Martin Y, Williams C C and Wickramasinghe H K 1987 Atomic force microscope-force mapping and profiling on a sub 100-Angstrom scale *J. Appl. Phys.* **61** (10)
- [14] Chu J, Itoh T, Lee C and Suga T 1997 Novel high vacuum scanning force microscope using a piezoelectric cantilever and the phase detection method *J. Vac. Sci. Technol. B* **15** (4)
- [15] Liang Y and Bonnell D A 1995 Observation of electric field gradients near field-emission cathode arrays *Appl. Phys. Lett.* **66** (9)
- [16] Nilsson L *et al* 2000 Scanning field emission from patterned carbon nanotube films *Appl. Phys. Lett.* **76** (15)
- [17] Martin Y *et al* 1988 High-resolution capacitance measurement and potentiometry by force microscopy *Appl. Phys. Lett.* **52** (13)
- [18] Zhang F *et al* 2004 *Japan. J. Appl. Phys.* at press